Distortion induced effects on the finesse of high-performance large-aperture Fabry-Perot etalon filters

J. Zhang[*], J. W. Arkwright, and D. I. Farrant

CSIRO Industrial Physics, PO Box 218, Lindfield, NSW 2070
AUSTRALIA
Ph: Int+ 612 9413 7064
[*]On secondment from the Harbin Institute of Technology
West Da-Zhi Street, Harbin, Heilongjiang, China.
john.arkwright@csiro.au

Abstract: The effect of thickness uniformity and distortion on the performance of large-aperture Fabry-Perot etalon filters is investigated. It is shown that for etalons currently being used for solar observation it is important to consider the effect of distortion due to mounting and to gravity when in use. It is further shown that the effects of distortion can be largely avoided by operating the etalon at or near normal incidence.

OCIS codes: (120.0120) Instrumentation, measurement and metrology; (220.4610) Optical Fabrication.

References and links

1. D. M. Rust, "Etalon filters," Opt. Eng. **33**, 3342-3348, 1994.
2. C. D. Prasad, S. K. Mathew, A. Bhatnagar, and A Ambastha, "Solar photospheric and chromospheric observations using a lithium niobate Fabry-Perot etalon," Exp. Astron. **8**, 125-133, (1998).
3. J. Arkwright, I. Underhill, N. Pereira, and M. Gross, "Deterministic control of thin film thickness in physical vapor deposition systems using a multi-aperture mask," Opt. Express **13**, 2731-2741 (2005).
4. V. Martínez Pillet, J. A. Bonet, M. Collados, et al., "The imaging magnetograph experiment for the SUNRISE balloon Antarctica project, Proc. SPIE **5487,** 1152-1164, 2004.
5. E. Hecht, *Optics*, (Addison-Wesley, Massachusetts, 1987).
6. J. Arkwright, D. Farrant, and J. Zhang, "Sub-nanometer metrology of optical wafers using an angle-scanned Fabry-Perot interferometer," Opt. Express **14**, 114-119 (2006).

1. Introduction

Large-aperture Fabry-Perot etalon filters fabricated from lithium niobate wafers are becoming increasingly popular for solar observation, for example for imaging of the hydrogen alpha (Hα) or helium (He I) absorption lines across the solar disk [1, 2]. Advances in etalon fabrication technology [3] now enable higher spectral selectivity to be achieved, and devices recently fabricated at CSIRO have included filters for tracking the Zeeman-split spectral line of iron (Fe I) in order to map the solar magnetic field [4]. With these increases in the required performance of the etalons, it is becoming necessary to consider the effect of variations in optical thickness of the etalon wafer due to distortion. Distortion can arise from incorrect mounting, residual stresses in the etalon substrate or coatings, or due to gravity if the etalon is mounted in the horizontal plane. Etalons should be mounted in a manner that constrains them from moving, while at the same time avoids stress that can cause physical distortion or refractive index perturbations.

This paper describes the effect of distortion on the performance of the etalon for spectral imaging purposes and shows that the effect of distortions increases with increasing angle of incidence. Because of this dependence on angle of incidence, for practical purposes the effect

#69918 - $15.00 USD Received 13 April 2006; revised 2 June 2006; accepted 6 June 2006

of distortion can be ignored as long as the etalon is operated at or near normal incidence. Results are presented for solid etalons, although the analysis is also applicable to air-spaced etalons in which the substrates forming the mirror surfaces are distorted.

2. Theory

For a solid Fabry-Perot etalon, high-reflectivity coatings are deposited on the wafer, with the coatings forming mirrors and the wafer acting as a spacer. The transmission of Fabry-Perot etalon filters is described by the Airy function [5]:

$$T(d,R,\lambda,\theta_i)=\frac{1}{1+\left(4R/(1-R)^2\right)\sin^2(2\pi n_i d\cos(\theta_i)/\lambda)}, \qquad (1)$$

where R is the reflectivity of the etalon mirrors (assumed equal), d is the physical separation between the mirrors, n_i is the refractive index of the medium between the mirrors, λ is the wavelength of the incident illumination, and θ_i is the angle between the normal to the surface of the etalon and the transmitted ray inside the etalon. To match the function to observable values, the internal angle is usually converted to the external angle of incidence, θ_e, using Snell's law:

$$\theta_e=\sin^{-1}\left(\frac{n_i}{n_e}\sin(\theta_i)\right), \qquad (2)$$

where n_e is the refractive index of the external medium, usually set to 1 if the etalon is in air.

At a given wavelength, peak transmission occurs when the argument of the sine function in Eq. (1) is equal to an integer multiple of π, and so when used for imaging of a selected atomic transition across the solar disk it is important to control both optical thickness and local angle of incidence in order to optimise transmission across the full aperture of the device. For example, if a relative transmission of >80% is required for all points across the aperture, then the physical thickness of a nominally 280 μm thick, z-cut lithium niobate etalon with a refractive index of 2.28, at a wavelength of 632.8 nm, and mirror reflectivity of 90%, must be controlled to within 1.2 nm. This is true for all angles of incidence; however, the acceptable variation in angle across the wafer caused by distortion is itself a function of the mean angle of incidence. The dependence of the optical thickness with internal angle is given by $n_i d\cos(\theta_i)$ and therefore, from Eq. (2), the effect increases with increasing external angle of incidence. For example, the effect of a 0.1° change in external angle equates to a thickness variation of only 0.08 nm at normal incidence but at 4° this increases to 6.6 nm. Furthermore, the effect is only of significance for distortion angles in the plane of incidence of the etalon. This can be readily deduced by considering the geometry of the incoming beam and the local plane of the etalon, and is confirmed experimentally in Section 4.

Whereas the variation in physical thickness can be controlled during fabrication of the etalon [3], the variation in local angle of incidence is dependent on the distortion of the etalon. The following Sections will describe the effect of distortions induced by incorrect mounting and also due to gravity.

3. Etalon measurement

The thickness variation maps of the etalon presented in this work were measured using an angle-scanning rig with sub-nanometre thickness resolution [6]. To determine the full thickness profile of the etalon the thickness variation map is added to the mean wafer thickness measured independently using a digital dial gauge. The distortions applied to the etalon, and those due to gravity, were measured using the laser deflectometer shown in Fig. 1. With reference to Fig. 1, a 1 mm diameter beam from a laser illuminates a spot on the etalon,

#69918 - $15.00 USD Received 13 April 2006; revised 2 June 2006; accepted 6 June 2006

which is then reflected back onto a CCD camera array. The etalon is moved laterally in one direction and the distortion is calculated from changes in the spot position on the CCD array.

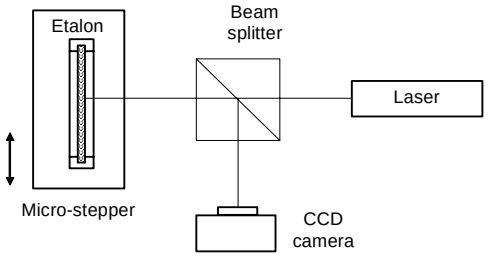

Fig. 1. Schematic of the laser deflectometer used to measure the distortion of the etalon wafers.

Finesse is often used as a measure of etalon performance [4]. For a small point on an etalon, or for a large area of a perfectly uniform etalon, the finesse approaches the reflective finesse, $F_R = \pi R^{1/2} / (1-R)$. In practice, the effective, or measured, finesse of the device across its full working aperture is lower as a result of surface roughness, surface figure, and distortion. The effective finesse measured at 96% reflectivity is used for comparative purposes throughout this paper. The effective finesse is determined by setting the reflectivity to the desired value and calculating the wavelength-dependent transmission functions of each sub-aperture using the local values of thickness and angle of incidence. A 128 x 128 array of sub-apertures covering the full aperture of the etalon is usually sufficient to give an acceptable result. The effective transmission function is then found from the average of all the sub-aperture transmission functions. The effective finesse is found from this composite transmission function using the following relationship:

$$F_e = \frac{FSR}{FWHM_e}, \tag{3}$$

where the *FSR* (Free Spectral Range) is the separation in wavelength between successive wavelength peaks, and the $FWHM_e$ (effective Full-Width Half-Maximum) is the width of one of the composite transmission peaks of the averaged transmission function measured at 50% of the peak, as is shown in Fig. 2. Figure 2 also shows an ideal transmission function from a uniform, undistorted etalon having a reflectivity of 96%. For high-performance etalons with clear apertures of 50-60 mm, the effective finesse can range from 20 to >50 [1, 3].

#69918 - $15.00 USD Received 13 April 2006; revised 2 June 2006; accepted 6 June 2006

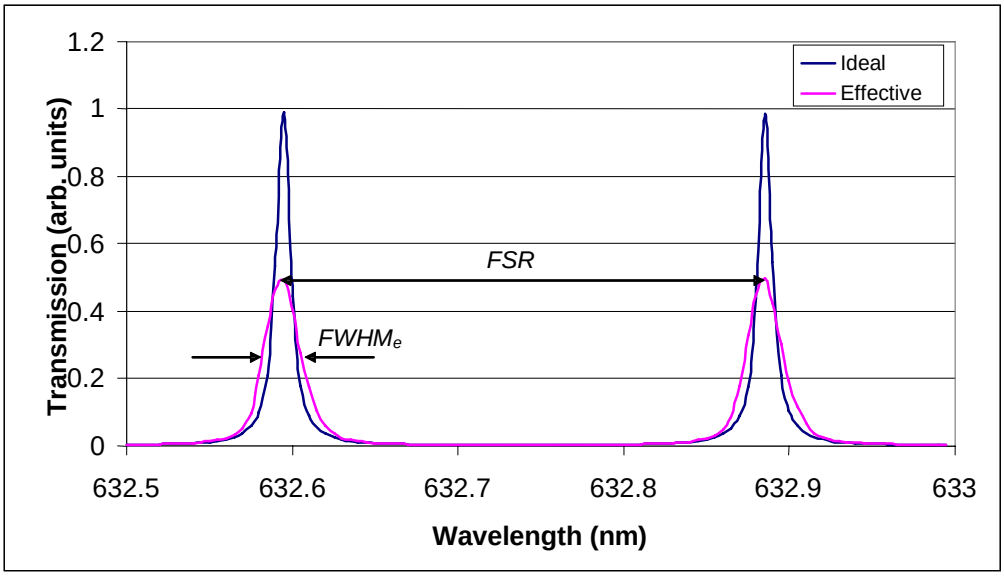

Fig. 2. Ideal and effective transmission functions of a large aperture etalon indicating the *FSR* and $FWHM_e$ used to calculate the effective finesse.

4. Results

The undistorted etalon thickness variation map is shown in Fig. 3, with a clear aperture of 63 mm and nominal thickness of 223 μm. This map was measured with the etalon mounted in the vertical plane, by scanning the etalon in angle around one of the symmetric first order fringes [6]. This fringe had maximum transmission at a mean angle of incidence of 3.94°. Using this thickness variation map and a reflectivity of 96% predicts an effective finesse of 37.4. Given *FSR* = 0.366 nm at a wavelength of 632.8 nm, then $FWHM_e$ = 9.8 pm, which is the approximate width of a Zeeman-sensitive solar spectral line [4].

To measure the effects of distortion, etalon was then purposely distorted by inserting four aluminium foil tabs into the etalon mount and then re-measured using the same order fringe. The locations of the aluminium tabs and the re-measured map are shown in Fig. 4. Comparing Figs. 3 & 4 shows that the distortion of the etalon creates a difference in measured thickness of up to 19 nm across the aperture of the etalon. In this instance the etalon has an effective finesse of 14.

To confirm that the measured effective finesse can be simulated by applying the distortion-induced perturbation to the local angle of incidence perpendicular to the axis of rotation of the etalon, the distortion of the etalon was measured using the laser deflectometer. The peak deviation from flatness was 36 μm in the horizontal direction and 10 μm in the vertical direction. The measured horizontal perturbation to the nominal 3.94° angle of incidence was applied numerically to each element of the etalon shown in Fig. 3. The difference function was taken between the distorted and the numerically distorted maps and the resultant error function agreed with that taken from the measured values to within ±1 nm peak-to-valley. The etalon was then rotated 90° clockwise and re-measured. This time the horizontal distortion effect was removed numerically from the measured map, which was then compared to the map shown in Fig. 3. Again, the maps agreed to within ±1 nm, demonstrating that only distortions in the plane of incidence are of significance.

#69918 - $15.00 USD Received 13 April 2006; revised 2 June 2006; accepted 6 June 2006

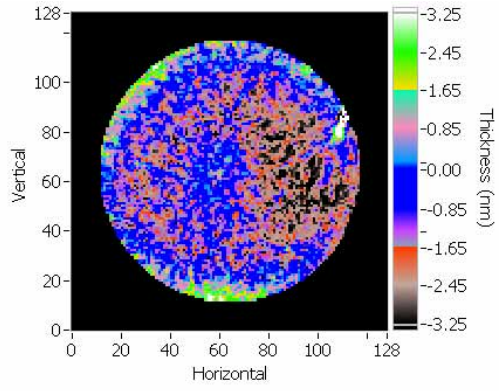

Fig. 3. Thickness variation map of the undistorted etalon, measured while mounted in the vertical plane. Horizontal and vertical axes are in pixel units (1 pixel ≈ 0.6 mm).

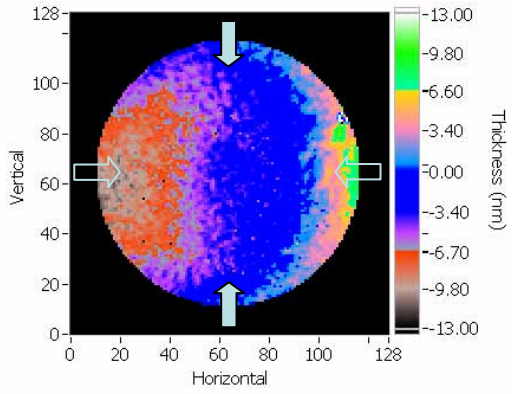

Fig. 4. Thickness variation map of the physically-distorted etalon measured while mounted in the vertical plane, at a mean angle of incidence of 3.94°. The locations of the aluminium tabs used to distort the etalon are also indicated. The horizontal pair of tabs were positioned behind the etalon and the vertical pair were in front of the etalon to induce the required distortion. Horizontal and vertical axes are in pixel units (1 pixel ≈ 0.6 mm).

This assumption was then used to determine the effect of gravity on the etalon when mounted in the horizontal plane. Since it was not possible to re-mount the angle scan rig to directly measure the etalon in the horizontal plane, the laser deflectometer was used to measure the gravity-induced distortion. The etalon was held loosely so that the edges were not constrained by the mount and the etalon distortion was measured along the axis perpendicular to the axis of rotation in both vertical and horizontal planes. These distortion functions are shown in Fig. 5. Using the distortion measured with the etalon in the horizontal plane, a distorted thickness map was again generated from Fig. 3 for an angle of incidence of 3.94° and is shown in Fig. 6. In this instance, the gravity-induced distortion creates a mean change in the thickness variation of 4.5 nm and reduces the effective finesse to 33.3.

#69918 - $15.00 USD Received 13 April 2006; revised 2 June 2006; accepted 6 June 2006

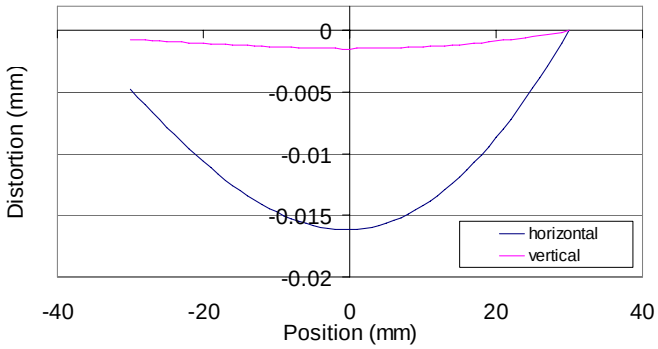

Fig. 5. Gravity-induced distortion functions, measured with the etalon held in vertical and horizontal planes

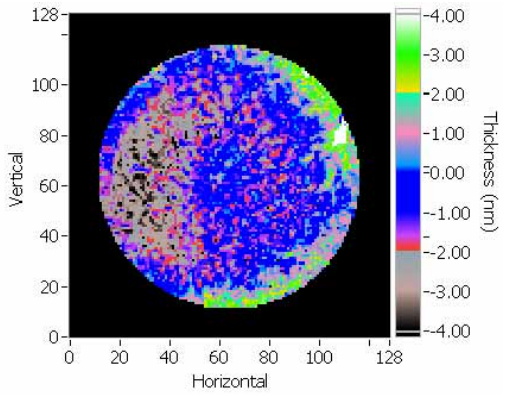

Fig. 6. Thickness variation map of the numerically-distorted etalon in the horizontal plane using the measured distortion due to gravity at an angle of 3.94°. Horizontal and vertical axes are in pixel units (1 pixel ≈ 0.6 mm).

5. Angular dependence

As mentioned in Section 2, the effect of distortion is itself a function of mean angle of incidence. This angular dependence provides a means of managing the effect of distortion on etalon performance. Since the etalons are fabricated from lithium niobate, the electro-optic or thermo-optic nature of the material can be used to tune the etalon to give peak transmission at normal incidence so that the effects of distortion are minimised. This can be simulated in the manner of Fig. 6, except with a mean angle of incidence of 0°. That is, modifying the measured thickness map shown in Fig. 3 using the measured gravity-induced angular perturbation at a mean angle of incidence of 0°. The calculated effective thickness variation differs from that of the undistorted etalon by less than 0.03 nm peak-to-valley and the effective finesse is fully recovered to the original value of 37.4, demonstrating that the effect of distortion is removed by operating at normal incidence.

6. Conclusions

It has been shown that the performance of high-finesse large-aperture etalons is degraded by distortions of the etalon wafer. Even the effect of gravity-induced sag can have a significant effect if the etalon is operated at angles of incidence of a few degrees. However, the effect of distortion-induced degradation in performance can be minimised by operating the etalon at or

#69918 - $15.00 USD Received 13 April 2006; revised 2 June 2006; accepted 6 June 2006

near normal incidence. For lithium niobate devices this can be achieved by tuning the device to give maximum transmission at normal incidence using either the electro-optic or thermo-optic properties of the material.

Acknowledgments

This paper is dedicated to our colleague and friend Associate Professor Jun Zhang who lost her life shortly after this work was completed. She brightened the life of all who knew her.

The authors would like to thank the Harbin Institute of Technology for supporting Jun Zhang during her secondment to CSIRO.

The authors would like to thank Wayne Stuart and Edita Puhanic from the Australian Centre for Precision Optics, at CSIRO Industrial Physics for preparing the lithium niobate etalons used for this work.

#69918 - $15.00 USD Received 13 April 2006; revised 2 June 2006; accepted 6 June 2006